

A Study of Neutrons in the Halo of Neutral Beam

Atsushi Takehashi

High Energy Physics Group

Department of Physics at Osaka University

February 14, 2006

Abstract

We measured the momentum spectrum of the neutrons that were produced by π^+ 's and protons hitting a 1.2 interaction length Pb.

The momentum distribution has a peak at about 50 MeV/c.

The number of neutrons per incident particle per unit solid angle increases as the angle from the beam axis increases from 0 to 1 radian.

The Geant3 simulation gives 0 ~ 20 % and 30 ~ 60 % higher overall rate than data for π^+ 's and protons, respectively. The momentum spectrum generated by the simulation is softer, and peaked at lower momentum.

We believe that the difference comes from the hadronic interaction cross section used in the GEANT3 simulation.

Acknowledgement

I would like to thank T.Hara, M.Yamaga for their invaluable advice on physics and experimental technique.

My special thanks go to K.Sakashita, E.Iwai, S.Kajiwara who gave me invaluable advice as members of this experiment. I enjoyed having many chats with them in my research life.

I also owe a lot to the members of the Yamanaka Taku Group at Osaka University for the good companionship and encouragement K.Kotera, H.Miyake, have given me great deal of help proceed my research. I would like to thank M.Kawaguchi. Their help and support for my research life must also be mentioned here.

Finally, I would like to thank Taku Yamanaka. He taught me physics, experimental technique, analysis and more. I am sure this thesis did not exist without his help and advice. Even my interest in high energy physics may come from him. I had a wonderful time with him and enjoyed a lot of talks about not only physics but also natural science, computer, and life.

Contents

1	Introduction	7
1.1	Decay of $K_L \rightarrow \pi^0 \nu \bar{\nu}$	7
1.2	Beam halo in $K_L \rightarrow \pi^0 \nu \bar{\nu}$ experiment	8
1.3	Motivation	8
1.4	Overview	9
2	Experiment	10
2.1	Overview of the experiment	10
2.2	Beam and target	11
2.3	Detector elements and layout	11
2.3.1	Neutron Detector	11
2.3.2	Veto counters	11
2.3.3	TOF counters	12
2.3.4	Gas Cherenkov counters	12
2.3.5	Finger counter	12
2.4	Trigger	12
2.5	Run summary	12
3	Detector calibration and correction	14
3.1	Neutron detector	14
3.1.1	Time walk correction	14
3.1.2	TDC calibration	14
3.1.3	ADC calibration	15
4	Event selection	17
4.1	Gas cherenkov counter	17
4.2	TOF counter	17
4.2.1	p/ π^+ separation	17
4.3	Charge veto counter	17
4.3.1	Charged particle cut	17
4.4	Neutron detector	18
4.4.1	TOF cut	18
5	Result	19
5.1	The angle distribution	19
5.2	Momentum distribution	19
5.3	A difference between data and MC	19
6	Discussion	23
6.1	Difference between data and MC	23

CONTENTS 4

7 Conclusion 24

List of Figures

1	The Z penguin and W-box diagrams which contribute to the decay $K_L \rightarrow \pi^0 \nu \bar{\nu}$	7
2	A sample geometry of target and collimators.	9
3	A brief sketch of detector.	11
4	The correlation between the ADC counts and TDC counts of the neutron detector before (left) and after (right) the time-walk correction.	15
5	The plot shows the distribution of TDC(NC) - TDC(S1) for a 2.0 GeV/c beam run. The peaks around the -1200 ch and -1100 ch correspond to the π^+ and the proton, respectively.	15
6	The plot shows TDC(NC) - TDC(S1) vs. the reciprocal of the speed of beam particles. We fitted points in this plot with a linear function. We used nine momentum conditions for this plot. 0.5 GeV/c, 0.6 GeV/c, 0.7 GeV/c, 0.8 GeV/c, 0.9 GeV/c, 1.0 GeV/c, 1.2 GeV/c, 1.5 GeV/c, 2.0 GeV/c. We used protons and π^+ 's above 0.6 GeV/c and only π^+ 's for 0.5 GeV/c.	16
7	The distribution of the energy deposited by 0.5 GeV/c π^+ in the neutron detector for GEANT 3 simulation (left) and data(right).	16
8	The plot shows the distribution of TDC(S2) - TDC(S1). The beam momentum is 1.0 GeV/c for this plot.	17
9	The left and right plots shows the distribution of TDC(Pb~NC) for π^+ 's and protons incident on the Pb target, respectively. We used the data for $x_0 = -10$ cm for these plots.	18
10	The angular distributions of neutrons for incident π^+ (left) and protons (right). Black circles show the simulation data and red circles show the MC data.	20
11	The momentum distributions of neutrons for incident π^+ (left) and protons (right). The top to bottom plots show the distributions at $x_0 = -10, -20, -50$ and -70 cm. The black line shows the experimental data and the red line shows the MC data. The number of MC events is normalized the total number of events in data.	21
12	The data/MC ratio of the neutron momentum spectrum for incident π^+ (left) and proton(right).	22

List of Tables

1	The size of the detector.	10
2	A summary of main runs.	13
3	A summary of calibration runs	13
4	The number of detected neutrons and incident particles for incident π^+ 's and protons	19

1 Introduction

1.1 Decay of $K_L \rightarrow \pi^0 \nu \bar{\nu}$

The rare decay $K_L \rightarrow \pi^0 \nu \bar{\nu}$ is a good window to determine the η parameter, where η is the imaginary parts of Kobayashi-Maskawa matrix. As shown in Fig. 1, this decay is governed by short-distance transition current and occurs almost entirely from the direct CP violation, as described below.

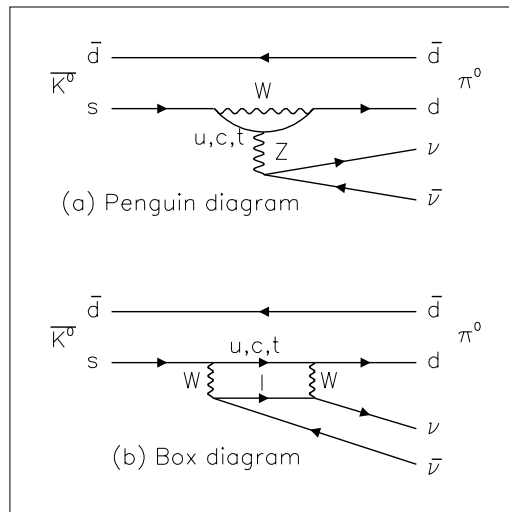


Figure 1: The Z penguin and W-box diagrams which contribute to the decay $K_L \rightarrow \pi^0 \nu \bar{\nu}$

The amplitude for $K_L \rightarrow \pi^0 \nu \bar{\nu}$ can be written as

$$A(K_L \rightarrow \pi^0 \nu \bar{\nu}) \simeq \frac{1}{\sqrt{2}} [A(K^0 \rightarrow \pi^0 \nu \bar{\nu}) - A(\bar{K}^0 \rightarrow \pi^0 \nu \bar{\nu})] , \quad (1)$$

Since top quark can be in an intermediate state(Fig. 1), this decay involves to the V_{td} and V_{ts} . Using the Wolfenstein's parameterization,

$$A(K_L \rightarrow \pi^0 \nu \bar{\nu}) \propto V_{td}^* V_{ts} - V_{ts}^* V_{td} \sim 2i\eta . \quad (2)$$

Thus, we can see that the branching ratio of $K_L \rightarrow \pi^0 \nu \bar{\nu}$ is proportional to η^2 , and its measurement determines the η parameter.

The branching ratio can be calculated [4, 5] as

$$BR(K_L \rightarrow \pi^0 \nu \bar{\nu}) = 1.94 \times 10^{-10} \eta^2 A^4 \chi^2(x) \quad (3)$$

where $x = m_t/m_W$, $\chi \sim x^{1.2}$, and A is a CKM parameter in Wolfenstein parameterization. The theoretical estimate of this branching ratio is $\cong 3.0 \times 10^{-11}$ based on the current knowledge of CKM parameters [4, 5]. Due to the uncertainties on the CKM parameters, these predictions still contain an error of $\cong 2 \times 10^{-11}$. The best published limit for the $K_L \rightarrow \pi^0 \nu \bar{\nu}$ decay is 5.9×10^{-7} (90%CL) from E799-I at Fermi National Accelerator Laboratory (FNAL)[6]. The theoretical uncertainty on the relation between $BR(K_L \rightarrow \pi^0 \nu \bar{\nu})$ and η , that is the uncertainty in $A^4 \chi^2(x)$ in equation (3), has a magnitude of a few percent[4]. Therefore, by measuring the branching ratio of $K_L \rightarrow \pi^0 \nu \bar{\nu}$, we can directly determine the CKM parameter η with a high accuracy.

1.2 Beam halo in $K_L \rightarrow \pi^0 \nu \bar{\nu}$ experiment

We are planning to measure the branching ratio of $K_L \rightarrow \pi^0 \nu \bar{\nu}$ decay at J-PARC. J-PARC is a new accelerator project in Japan which produces MW-class high power proton beam. It is suitable for the $K_L \rightarrow \pi^0 \nu \bar{\nu}$ experiment because of its high energy(30GeV) and high intensity ($< 3.3 \times 10^{14}$ proton per pulse) beam which can produce many high energy K_L 's.

In J-PARC $K_L \rightarrow \pi^0 \nu \bar{\nu}$ experiments, we bombard protons on the target to produce K_L . Neutral beam line consists of three elements. First is a magnet to sweep out charged particles. Second is an absorber to reduce the n/K_L ratio. The last is a collimator to make a narrow beam with a sharp edge.

Figure 2 shows a sample geometry of target and collimators. The collimator has the conic hole whose apex is at the center of the target.

Besides K_L 's and neutrons in the beam, there are some neutrons outside the beam. They are called beam halo neutrons, and there are two kinds of them. One of them is those which passed through the long distance in the collimator. Another is those which were produced by neutrons hitting the edge of the hole of the collimator. By using a thick collimator, the number of penetrating neutrons can be reduced, but the neutrons from the edge still survive.

1.3 Motivation

For designing the collimator, we need to know the yield and momentum spectrum of neutrons that comes off the edge of the collimator. It is important

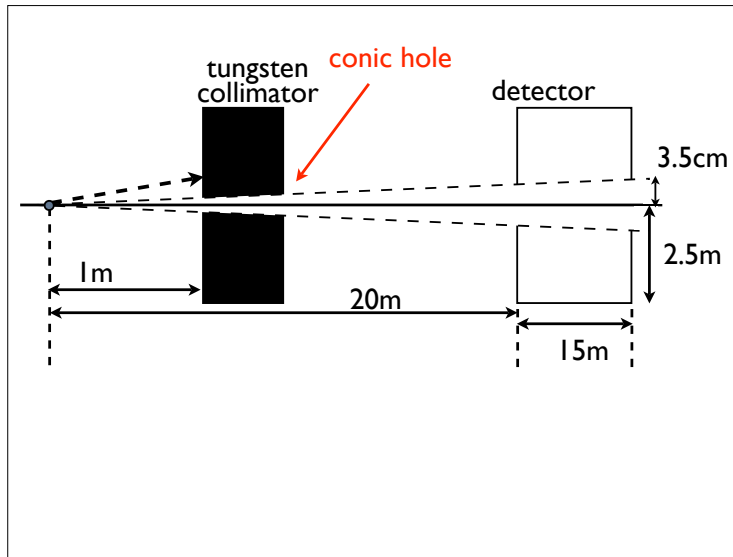


Figure 2: A sample geometry of target and collimators.

to measure them experimentally, since hadronic interaction is not easy to simulate.

When neutrons interact in the material, they generate π^+ 's and protons, and these π^+ 's and protons generate the neutrons. According to Monte Carlo simulation, the yield and momentum spectra of the neutrons are similar between incident π^+ 's, protons, neutrons.

Therefore, we ran an experiment by bombarding π^+ 's and protons near the edge of a Pb target and directly measured the distribution of the direction and the momentum of neutrons which came off the Pb target. We will compare the result with simulation.

1.4 Overview

Chapter 2 describes the details of detector and run condition. Chapter 3 describes the calibration and the correction of the detectors. Chapter 4 describes the event selection to suppress backgrounds. In Chapter 5 and 6, we will present the result and discussion, respectively. Chapter 7 gives the conclusion of this study.

2 Experiment

2.1 Overview of the experiment

We used the π^2 beam line at the KEK (High Energy Accelerator Research Organization). The 12 GeV primary protons bombarded the internal target in the main ring. The secondary particles were bent with the bending magnet and brought to the π^2 area. Beam momentum ranged from 0.5 GeV/c to 4. GeV/c.

Table 1: The size of the detector.

S1	10 cm \times 10 cm \times 1 cm plastic scintillator.
S2	9 cm \times 14 cm \times 1 cm plastic scintillator.
GC1,GC2	90 cm gas Cherenkov counter.
F1	1.5cm \times 1.5 cm \times 1 cm plastic scintillator.
CV1	17 cm \times 17 cm \times 0.5 cm plastic scintillator.
CV2	20 cm \times 40 cm \times 0.5 cm plastic scintillator.
NC	12.7 cm ϕ \times 12.7 cm long liquid scintillator.

The secondary beam was focused on a $1.2 \lambda_I$ thick Pb target. Figure 3 shows a schematic drawing of all the elements in our detector. Table 1 shows the size of detectors elements.

First, let us define our coordinate system and a variable. We set the origin at the intersection of the beam axis and the downstream surface of the Pb target. We choose the Z axis along the beam line and the X axis as shown in Figure 3.

We measured neutrons with a liquid scintillation counter. We measured the momentum of neutrons using the time of flight (TOF) between the Pb target and neutron detector.

Apart from the main run, we had calibration runs. In this run, we removed Pb target and set the neutron counter in the beam line.

We used 1GeV/c beam for the main run and 0.5GeV/c \sim 2.0GeV/c beam for the calibration runs.

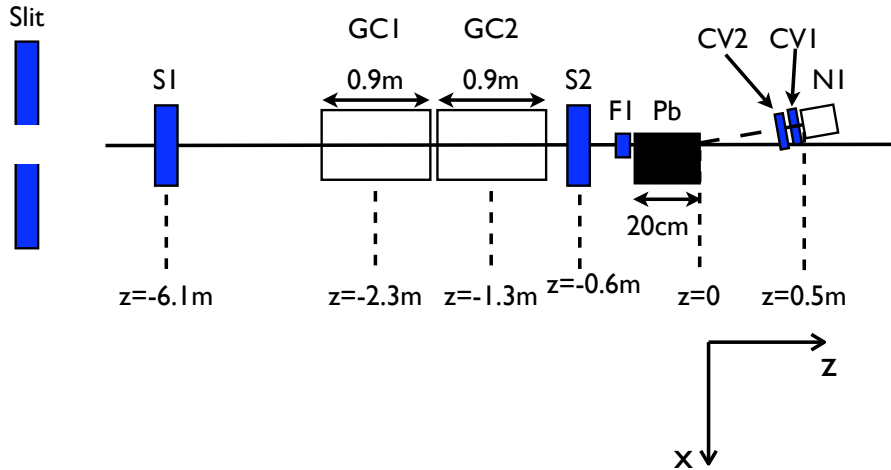


Figure 3: A brief sketch of detector.

2.2 Beam and target

The target in the secondary beam line is made of Pb. The size of the target is 15 cm (x) \times 20 cm (y) \times 20 cm (z , $1.17 \lambda_I$). The Pb target was aligned so that the beam center hits 1cm inside the edge.

2.3 Detector elements and layout

2.3.1 Neutron Detector

In order to measure neutrons which were emitted from the target, we used a neutron detector in the experiment.

The neutron detector consist of 1.6 liters of NE213 liquid scintillator filled in a cylindrical vessel with 5 inch $\phi \times$ 5 inch long (12.7 cm $\phi \times$ 12.7 cm long). The neutron detector is equipped with a 5 inch Hamamatsu R1250 phototube. Here, we define (x_0, y_0, z_0) as the coordinate of the center of the front face of the neutron detector. We set the neutron detector as $z_0 = 50$ cm. We changed x_0 as 10 cm, 20 cm, 50 cm and 70 cm. The center line of the neutron detector was always aligned to point the origin of the coordinate.

2.3.2 Veto counters

Two charge veto counters (CV1 and CV2) were placed in front of the neutron counter to detect charged particles entering the neutron counter from the Pb target.

The centers of CV1 and CV2 were aligned to be on the line connecting the coordinate origin and the center of the neutron detector. The CV1 and CV2 were aligned to be parallel to the front face of the neutron detector.

2.3.3 TOF counters

We measured the TOF of particles in the secondary beam with two scintillation counters, S1 and S2, to identify the particles. Each counter is equipped with Hamamatsu H2431 phototubes on two sides. We will define TDC(S1) as the average of the TDC counts of the two phototubes on S1, and similarly for S2.

2.3.4 Gas Cherenkov counters

We discriminated π^+ 's from positrons with two gas Cherenkov counters. Each counter is 90 cm long. The gas in these counters was air at 1 atm.

2.3.5 Finger counter

We placed a finger counter (1.5 cm (W) \times 1.5 cm (H) \times 1.0 cm (D)) at $x = y = 0$, $z = -20$ cm and confirmed that particles in beam hit the Pb target near the edge.

2.4 Trigger

The trigger condition was $S1 \cdot S2 \cdot F1$, where each element is a discriminated signal from each counter.

2.5 Run summary

The data was taken from November 29 (2005) to December 5 (2005). Table 2 and 3 summarize the number of collected events in main runs and calibration runs, respectively.

Table 2: A summary of main runs.

-x0(cm)	number of event
10	220887
20	1228208
50	6011644
70	8640823

Table 3: A summary of calibration runs

beam momentum(GeV/c)	number of event
0.5	31060
0.6	20252
0.7	21083
0.8	20418
0.9	23598
1.0	25569
1.2	24287
1.5	22813
2.0	25442

3 Detector calibration and correction

The TDC for the neutron detector was calibrated by using beam particles in the calibration run. The gain of an ADC channel for the neutron detector was calibrated by using a calibration run and simulation data.

The following sections will describe the details of the detector calibration and the time walk correction.

3.1 Neutron detector

3.1.1 Time walk correction

The plot on the left column in Figure 4 shows the correlation between ADC counts and TDC counts of the neutron detector for gamma-like events. We roughly selected them by TDC counts of the neutron detector and by the charged veto counters. Since there is a correlation between ADC counts and TDC counts for the neutron detector due to a time walk, we corrected the TDC counts of the neutron detectors. We fitted this correlation for the expression:

$$TDC_{fit} = C_1 \cdot (ADC)^{-1/2} - C_2 \cdot (ADC) + C_3$$

where C_1 , C_2 and C_3 are free positive parameters. Using the fitted C_1 , C_2 and C_3 , we corrected TDC value as:

$$TDC_{corr} = TDC_{raw} - C_1 \cdot (ADC)^{-1/2} + C_2 \cdot (ADC).$$

The plot on the right column in Figure 4 shows the distribution between ADC and TDC counts after the correction.

3.1.2 TDC calibration

We calibrated the TDC of the neutron detector by using the particles in the beam line, in the calibration data.

Figure 5 shows the distribution of TDC(NC) - TDC(S1). The peak around the -1200 ch and -1100 ch corresponds to the π and the proton, respectively. We fitted this distribution around each peak with Gaussian.

Figure 6 shows the mean values of the fitted Gaussian for TDC(NC) - TDC(S1) versus the reciprocal of the speed of beam particles. We fitted points in the plot with a linear function and obtained 45.77 ns / count.

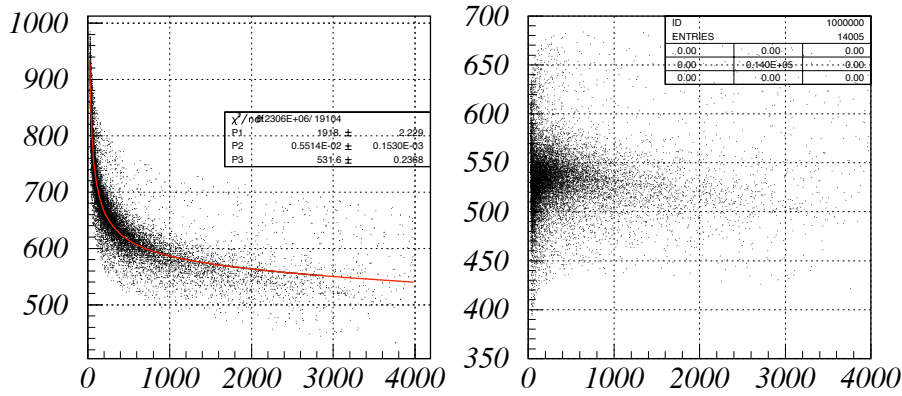


Figure 4: The correlation between the ADC counts and TDC counts of the neutron detector before (left) and after (right) the time-walk correction.

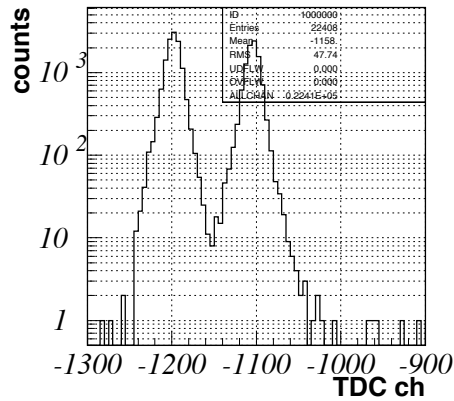


Figure 5: The plot shows the distribution of TDC(NC) - TDC(S1) for a 2.0 GeV/c beam run. The peaks around the -1200 ch and -1100 ch correspond to the π^+ and the proton, respectively.

3.1.3 ADC calibration

We calibrated the ADC of the neutron detector by comparing the energy deposited by π^+ penetrating the detector, between data and MC.

Figure 7 (left) shows the distribution of the energy deposited in the neutron detector calculated by the Geant3 Monte Carlo simulation. Figure 7 (right) shows the distribution of the deposited energy measured in the calibration run. We assumed the peak values of these distribution are the same, and obtained 8×10^{-3} MeV/count.

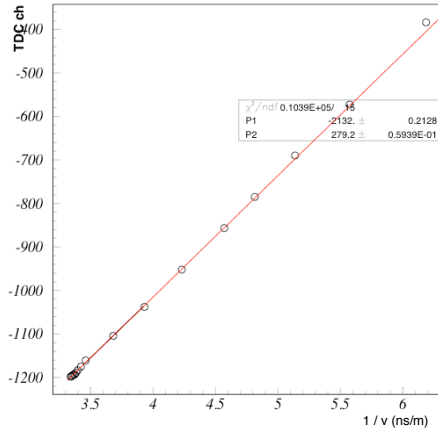


Figure 6: The plot shows TDC(NC) - TDC(S1) vs. the reciprocal of the speed of beam particles. We fitted points in this plot with a linear function. We used nine momentum conditions for this plot. 0.5 GeV/c, 0.6 GeV/c, 0.7 GeV/c, 0.8 GeV/c, 0.9 GeV/c, 1.0 GeV/c, 1.2 GeV/c, 1.5 GeV/c, 2.0 GeV/c. We used protons and π^+ 's above 0.6 GeV/c and only π^+ 's for 0.5 GeV/c.

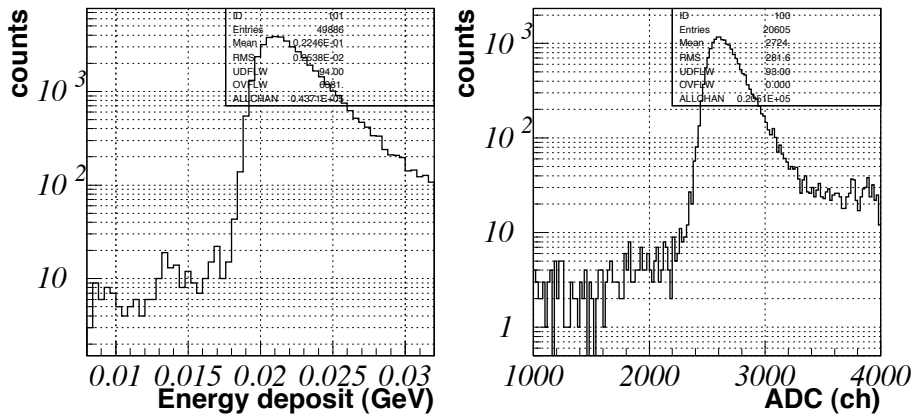


Figure 7: The distribution of the energy deposited by 0.5 GeV/c π^+ in the neutron detector for GEANT 3 simulation (left) and data(right).

4 Event selection

4.1 Gas cherenkov counter

We rejected e^+ in the beam with the gas Cherenkov counters.

In the analysis, we cut on the ADC and the TDC of two gas Cherenkov counters. We required the ADC counts to be less than $3\sigma_{ped}$ above the pedestal where σ_{ped} is width of the pedestal peak. We required the TDC to have no hits in a 100 ns time window.

4.2 TOF counter

4.2.1 p/π^+ separation

We distinguished between protons and π^+ 's with the TOF between S1 and S2. Figure 8 shows the distribution of the TDC value. We fitted this distribution for a Gaussian around the individual peak. We required the $TDC(S2) - TDC(S1)$ to be within 3 sigma of the mean values of the fitted Gaussian.

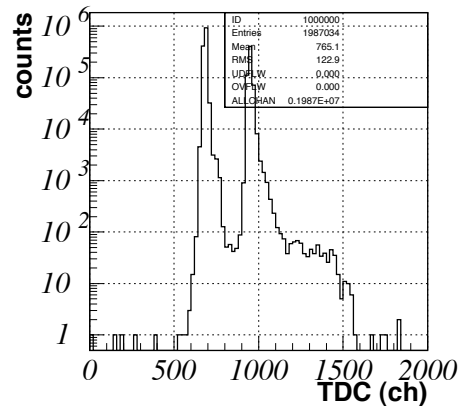


Figure 8: The plot shows the distribution of $TDC(S2) - TDC(S1)$. The beam momentum is 1.0 GeV/c for this plot.

4.3 Charge veto counter

4.3.1 Charged particle cut

We discriminated neutral particles from charged particles entering the neutron detector. We required the ADC counts to be less than $3\sigma_{ped}$, where σ_{ped} is width of the pedestal peak for a Gaussian. The TDCs were required to have no hits in 100 ns time window.

4.4 Neutron detector

We discriminated neutrons from photons by using the time-of-flight between the Pb target and the neutron counter.

4.4.1 TOF cut

First, we defined the TOF between the target and the neutron detector :

$$TOF(Pb \sim NC) = TOF(S1 \sim NC) - TOF(S1 \sim Pb),$$

where $TOF(S1 \sim NC)$ is the TOF between S1 and the neutron counter, and $TOF(S1 \sim Pb)$ is the TOF between S1 and the origin of the coordinate, calculated from the beam momentum and the mass of the selected particle.

Figure 9 shows the distribution for the TDC(Pb~NC). We fitted this distribution around peak at about $0 \sim 5$ ns for a Gaussian. In order to select neutrons, we required:

$$TOF_{corr} > (\mu_{photon} + 3\sigma_{photon}),$$

where μ_{photon} is the mean values of the fitted Gaussians for photons, and σ_{photon} is the standard deviations for photons, respectively.

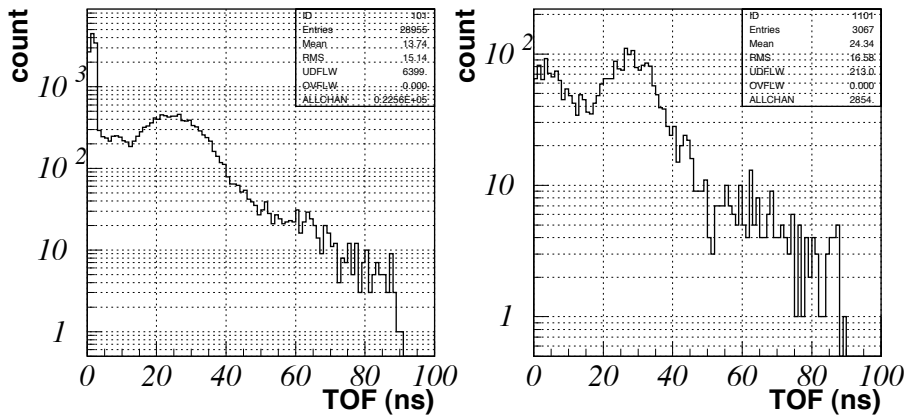


Figure 9: The left and right plots shows the distribution of TDC(Pb~NC) for π^+ 's and protons incident on the Pb target, respectively. We used the data for $x_0 = -10$ cm for these plots.

5 Result

In this section, we show the momentum and angle distributions for the neutrons produced at the Pb target and compare these distributions between data and Monte Carlo (MC) simulation. The MC sample was generated with Geant3 simulation code and analyzed in the same way as data.

5.1 The angle distribution

Table 4 shows the number of incident particles and the detected neutrons for each neutron counter position. Figure 10 shows the number of neutrons per incident particle normalized by the solid angle of the detector. The rate of the neutrons is higher at larger angle.

Table 4: The number of detected neutrons and incident particles for incident π^+ 's and protons

$x_0(cm)$	detected n / incident π^+	detected n / incident proton
-10	12378 / 1358941	2670 / 584491
-50	7254 / 756402	1479 / 313299
-70	7185 / 1029252	1403 / 413376
-20	13185 / 2560782	2441 / 1040342

5.2 Momentum distribution

Figure 11 shows the momentum distribution of neutrons measured with the TOF method. Each distribution has the peak at about 50 MeV/c.

5.3 A difference between data and MC

We compare the momentum distribution between data and MC in Fig 11. The peak momentum for MC is 10 MeV \sim 25 MeV lower than that of data. Also, the MC has softer momentum spectrum than data.

Figure 12 shows the ratio of data to MC for each momentum bin. The ratio is nearly constant at the momentum higher than 0.1 GeV/c, but decreases sharply as the momentum goes lower.

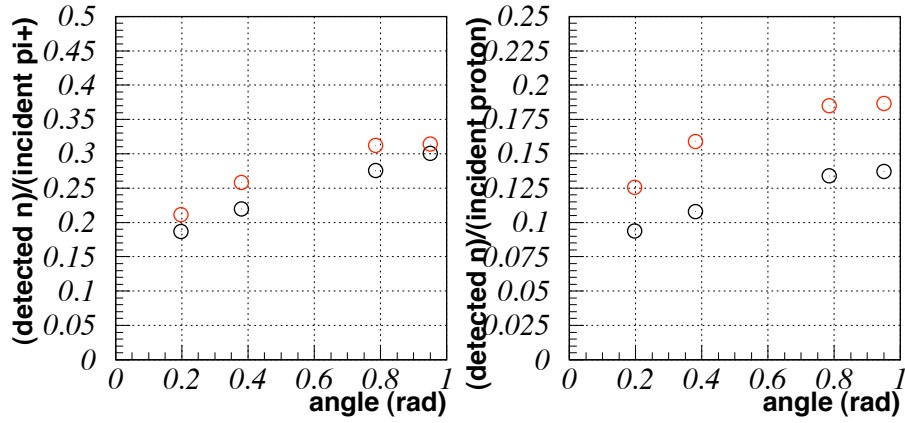


Figure 10: The angular distributions of neutrons for incident π^+ (left) and protons (right). Black circles show the simulation data and red circles show the MC data.

We also compare the number of neutrons per incident particle at each position as shown in Figure 10. The rate for MC is larger than data by 0 ~ 20 % for π^+ 's and 30 ~ 60 % for protons.

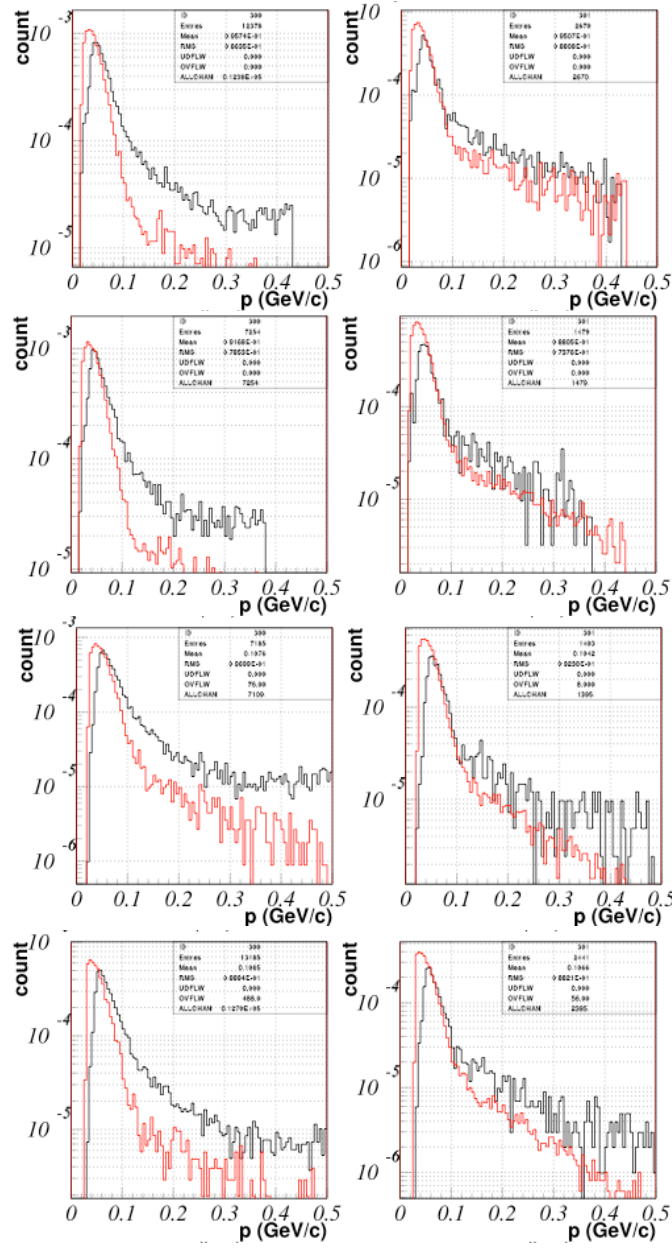


Figure 11: The momentum distributions of neutrons for incident π^+ (left) and protons (right). The top to bottom plots show the distributions at $x = -10, -20, -50$ and -70 cm. The black line shows the experimental data and the red line shows the MC data. The number of MC events is normalized the total number of events in data.

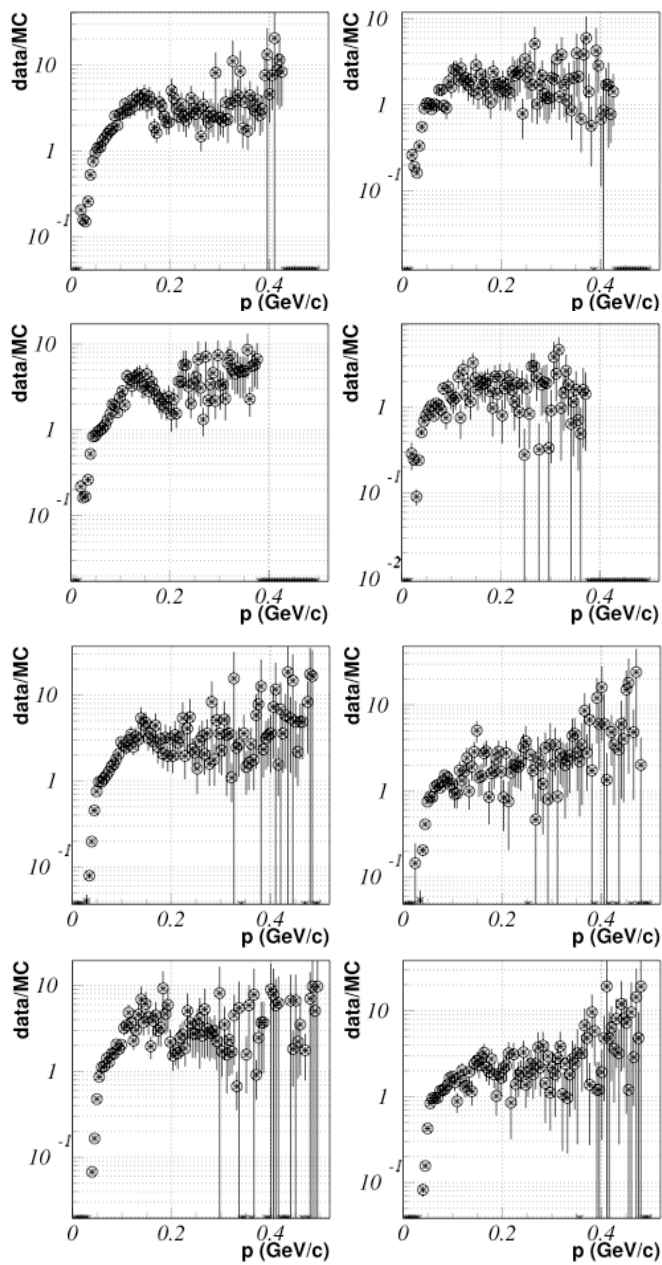


Figure 12: The data/MC ratio of the neutron momentum spectrum for incident π^+ (left) and proton(right).

6 Discussion

6.1 Difference between data and MC

We consider the cause for the difference between data and MC.

The first possibility is the time resolution of the neutron detector. However this just smears the distribution and does not move the peak momentum. Therefore, this is not the only cause.

We think that the main cause of the difference is in the simulator, most likely, in the cross section for hadronic interaction.

7 Conclusion

We measured the momentum spectrum of the neutrons that were produced by π^+ 's and protons hitting a 1.2 interaction length Pb.

Each momentum distribution has a peak at about 50 MeV/c.

The number of neutrons per incident particle per unit solid angle increases as the angle from the beam axis becomes larger from 0 to 1 radian.

The Geant3 simulation gives 0 ~ 20 % and 30 ~ 60 % higher overall rate than data for π^+ 's and protons, respectively. The momentum spectrum generated by the simulation is softer, and peaks at lower momentum.

We believe that the difference comes from the hadronic interaction cross section used in the GEANT3 simulation.

References

- [1] J. Cronin, V. Fitch *et al.*, Phys. Rev. Lett. **13**, 138 (1964).
- [2] M. Kobayashi and T. Maskawa, Prog. Theor. Phys. **49**, 652 (1973).
- [3] L. Wolfenstein, Phys. Rev. Lett. **51**, 1945 (1983).
- [4] A. Buras, Phys. Lett. **B333**, 476 (1994).
- [5] G. Buchalla and A. Buras, Phys. Rev. **D54**, 6782 (1996).
- [6] A. Alavi-Harati *et al.*, Phys. Rev. **D61**, 072006 (2000).